Modeling and Testing of a Biomimetic Flagellar Propulsion Method for Microscale Biomedical Swimming Robots

Bahareh Behkam and Metin Sitti, *Member, IEEE*

***Abstract*— Medical applications are among the most impactful areas of microrobotics. The ultimate goal of medical microrobots is to reach currently inaccessible areas of the human body and carry out a host of complex operations such as minimally invasive surgery (MIS), highly localized drug delivery, and screening for diseases at their very early stages. Miniature, safe and energy efficient propulsion systems hold the key to maturing this technology but they pose significant challenges. In this paper, authors propose a new type of propulsion inspired by the motility mechanism of prokaryotic microorganisms. The perfomance of these propulsive mechanism is estimated by modeling the dynamics of the motion. Analyzing key parameters such as linear velocity and efficiency, the optimum design of propulsion mechanism for miniatue robots is demonstrated. In order to validate the theoretical result for flagellar proplusion, a scaled up prototype of the swimming robot is fabricated and characterized in silicone oil using the Buckingham PI theorem for scaling. The proposed propulsion method is for the swimming robots which is intended to swim in low velocity biofluids. Potential target regions to use these robots include eyeball cavity, cerebrospinal fluid and the urinary system.**

Keywords– **Biomedical microrobotics, biomimetic robotics, swimming robots, flagellar motion.**

I. Introduction

MINIATURE swimming robots could be greatly beneficial for screening and treatment of many diseases. Due to their small size, microswimming robots operate in very small Reynolds (Re) numbers. Reynolds number is defined as the ratio of inertia forces to viscous forces and characterizes the fluid flow. A low Reynolds number infers that inertial forces are less significant or even negligible compared to viscous forces. Therefore, microscale swimmers in general experience drastically different hydro-dynamics compared to macroscale swimming robots. There are few biomimetic swimming robot, mostly fin-driven, developed [1-5]. Since fish-like biomimetic robots rely on inertial forces for propulsion, miniaturization will make them ineffective [1]. Another design was introduced by Ishiyama *et al*. at Tohoku University [5]. In this method an external magnetic field is used to rotate a small ferromagnetic screw in liquid. The advantages of this machine are that it does not require any power source or controller on the machine and it is not tethered which makes it very attractive for medical purposes. It has been demonstrated that this spiral type machine can swim in liquids of various viscosities in a broad range of Re numbers. However, speed limitation is the main disadvantage of this machine. For the frequency higher than the frequency which corresponds to the maximum acquirable speed, the rotation of the machine could not synchronize to the rotational frequency of the external field and the velocity decreased. Besides the speed limitation issue, there are other issues associated with the usage of a magnetic field: (1) Patients with pacemakers, metal implants and bullet wounds can not be subjected to magnetic fields. Magnetic force can pull on these objects, cutting and compressing healthy tissue. (2) Considering the low speed of the robot, the patient may be required to stay in the magnetic field for longer than the time allowed by FDA regulations. (3) Gradient fields can produce eddy currents in the patient and cause heating. This is not usually a concern in Magnetic Resonance Imaging (MRI), but it might become an issue if the robot is moving inside the body. Therefore, we propose a novel safe, miniature and energy efficient propulsion system potentially used for all patients with no restriction. Also, the proposed method does not subject the patients to the discomfort of staying in magnetic field for an extended period of time. Our proposed biomimetic propulsion concept is inspired by the peritrichous flagellation used by bacteria such as *E. Coli* and *S. Marcescens* [6-7], depicted in Fig. 1. The flagella of these cells are randomly distributed over the cell surface and each flagellar motor rotates independently of the others. Hydrodynamic interactions among flagella cause them to coordinate, coalescing and bundling behind the cell during swimming [8]. The flagellum is a propulsive organelle that includes a reversible rotary motor embedded in the cell wall, and a filament that extends into the external medium [9]. The filament is a long (~ 10 μm), thin (~ 20nm) helix (2.5

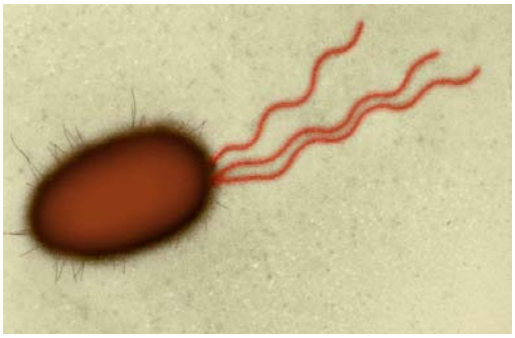

Fig.1. Transmission Electron Microscopy (TEM) image of *E. Coli* (x3515) "Image copyright Dennis Kunkel Microscopy, Inc. Used with permission"

Manuscript received March 15, 2005. This work was supported in part by ICES-DOWD fellowship.

B. Behkam is with the Mechanical Engineering Department, Carnegie Mellon University, Pittsburgh, PA 15213, USA (email: behkam@cmu.edu).

M. Sitti is with the Mechanical Engineering Department and Robotics Institute, Carnegie Mellon University, Pittsburgh, PA 15213, USA (phone: 412-268-3632; fax: 412-268-3348; e-mail: sitti@cmu.edu).

μm pitch, 0.5 μm diameter) that turns at speed of ~100 Hz [10]. For these microorganisms, $Re \approx 10^{-4}$ meaning viscous effects are dominant and inertial forces are insignificant. Therefore, this propulsion method can perform effectively even at very small scale and low Re numbers. This research work intends to investigate the potential for using prokaryotic flagellar motion for microrobotic propulsion.

II. METHODOLOGY

To develop an appropriate propulsion system, it is essential to understand the kinematics and dynamics of miniature swimming robots. Based upon the application that the miniature medical robot is designed for, the body of the robot can have diameter ranging from 800 μm to 8 mm. Assuming the biofluid that the robot will swim in has the property of water, *Re* number for swimming robot will vary in the range of 10^{-4}-100.

Based upon the size of the robot, we anticipate that either the Re of the robot or local Re of its propulsive components would be much smaller than 1. This regime of fluid flow is called stokes flow. Main characteristic of stokes flow are: (1) The viscous forces are dominant over the inertial force, and (2) Motion is time independent.

Biologists and mathematicians have extensively studied hydrodynamic of the microorganism swimming in stokes flow regime [11-12]. In this work we utilize the previously developed models and extend their findings in order to demonstrate the effective design for microscale robots.

III. MODELING

A. Low Reynolds Number Flow

Reynolds number is defined as:

$$Re = \frac{\rho V l}{\mu} \tag{1}$$

where ρ and μ are density and dynamic viscosity of the fluid, respectively. V is the flow velocity and l is the characteristic dimension of the object. For the microscale objects moving in water, due to the size of the object and fluid properties of water, $Re<<1$. For this type of flow Navier-Stokes equation reduces to:

$$\nabla p + \mu \nabla^2 U = 0 \tag{2}$$

where p is the pressure and U is the velocity. This equation is absent of any time dependent terms, signifying that the generated propulsion force only depends on the propeller's position. This infers any motion that completely retraces its own steps, like the flapping of fish's fin, will result in no net forward movement. The classic example is the motion of scallop. Scallop propels forward by slowly opening its hinge and then quickly closing it; if scallop were scaled down to be a few micrometers, this motion would result in periodic slight forward and backward motion with no net displacement.

To overcome this problem, organisms living in low Reynolds number regimes either have propulsive organelles with a handedness to them or move their propulsive organelles in an asymmetric fashion. For instance, *E. Coli*'s flagella have a helical structure, much like a corkscrew. This configuration produces patterns of motion that do not repeat the first half of the cycle in reverse for the second half, allowing the organisms to achieve movement in their environment.

B. Modeling of the flagellar motion

In 1955, Gray and Hancock [11] developed resistive force theory (RFT) for flagellar hydrodynamics analysis. This theory states that the normal, binormal and tangential components of drag force of any element of a slender body are proportional to the respective component of the local velocity with different proportionality constants. This theory is valid for the situation in which viscous effects dominate, i.e. Re<<1. Major restriction for applying this theory is that the radius of the curvature of the rigid body is large compared with body radius [12].

For the system depicted in fig. 2., the equations for conservation of linear and angular momentum are as follows:

$$\begin{aligned} LF_x + C_D U &= 0 \\ ALF_y + C_{D\Omega}\Omega &= 0 \end{aligned} \tag{1}$$

where F_x and F_y are the viscous forces in x and y directions. C_D and $C_{D\Omega}$ are the coefficient of drag and angular coefficient of drag of the head, respectively. L is the length of the flagellum and A is the amplitude. U is the linear velocity of the robot and Ω is the angular velocity of the head. The forces in x and y direction can be decomposed into the normal and tangential components:

$$\begin{aligned} F_x &= F_l \cos\theta - F_n \sin\theta \\ F_y &= F_l \sin\theta + F_n \cos\theta \end{aligned} \tag{2}$$

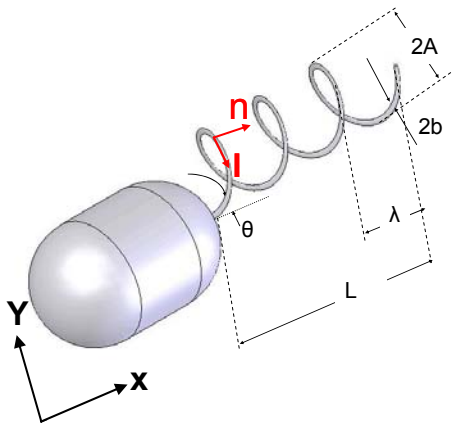

Fig. 2. Schematic of the microscale swimming robot

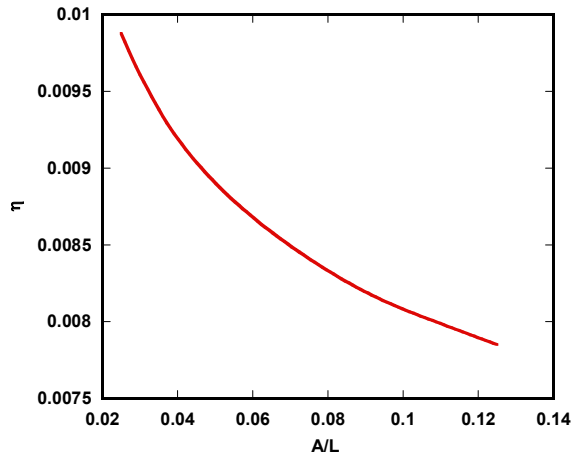

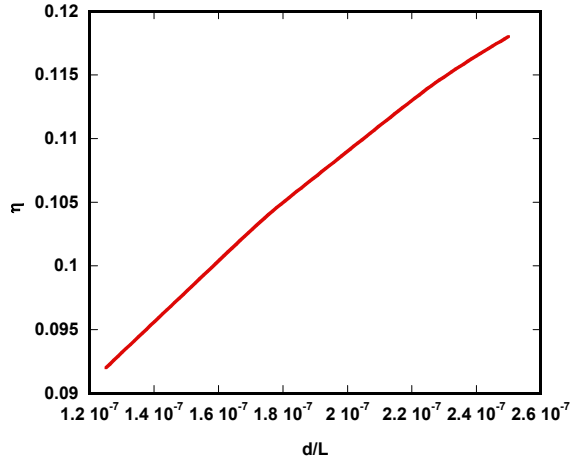

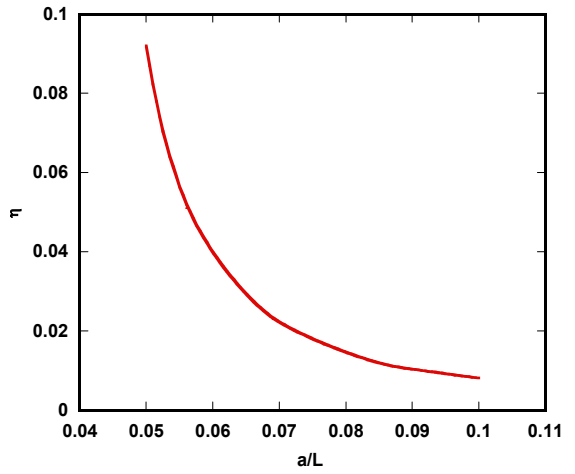

Fig.3. Efficiency of the robot as a function of non-dimensionalized geometrical parameters

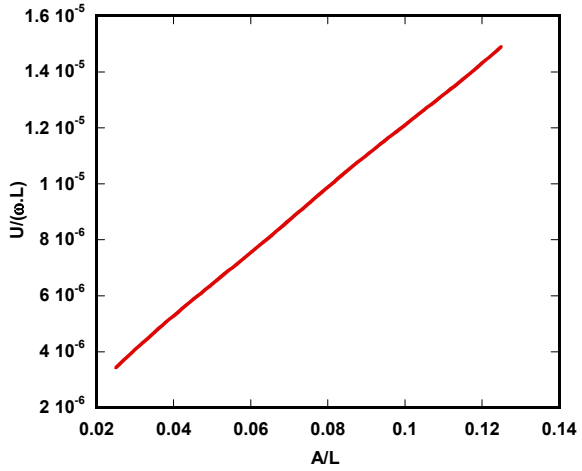

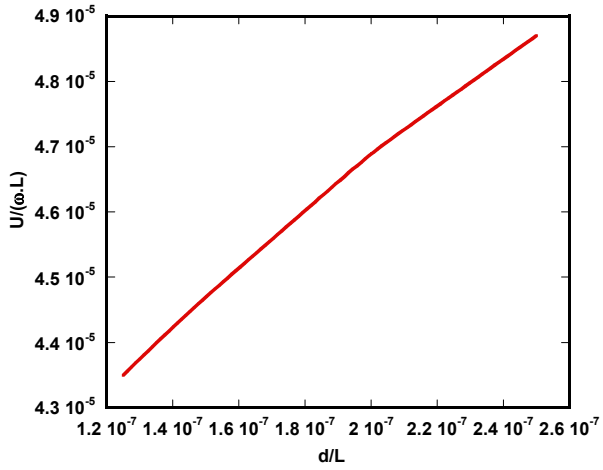

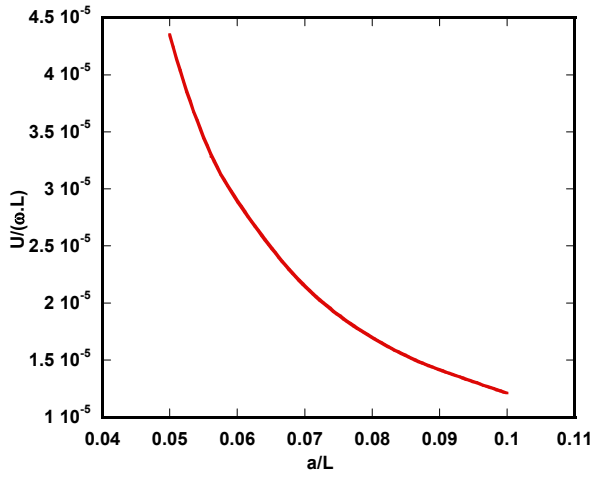

Fig.4. Non-dimensionalized velocity of the robot as a function of non-dimensionalized geometrical parameters

in which θ is defined by:

$$\tan\theta = \frac{\lambda}{2\pi A} \qquad (3)$$

where λ is the wavelength of the tail. Propulsive force in x direction, F_x, is required to overcome the drag force acting on the body of the robot. The viscous forces exerted on the tail in x and y direction can be written in terms normal and tangential forces. RFT demonstrates a relation between the

each component of the force and corresponding local velocity [11]:

$$\begin{aligned} \vec{f}_l(l) &= \mu C_l(l)\vec{V}_l(l) \\ \vec{f}_n(l) &= \mu C_n(l)\vec{V}_n(l) \end{aligned} \tag{4}$$

therefore:

$$\begin{aligned} F_l &= -C_l(U\cos\theta - \omega A\sin\theta) \\ F_n &= -C_n(U\sin\theta - \omega A\cos\theta) \end{aligned} \tag{5}$$

where Coefficients C_l and C_n are empirically derived for a single flagellum with both free ends[11]:

$$\begin{aligned} C_l &= \frac{2\pi\mu}{\ln(\frac{2\lambda}{b}) - \frac{1}{2}} \\ C_n &= \frac{4\pi\mu}{\ln(\frac{2\lambda}{b}) + \frac{1}{2}} \end{aligned} \tag{6}$$

Solving equations (1) through (6) simultaneously, propulsive force, required torque, linear velocity of the robot and angular velocity of the body is calculated. The thrust force is:

$$F = F_x.L \tag{8}$$

$$F_x = \omega A\sin\theta\cos\theta\{\frac{-LC_nC_l + C_nC_D - LC_l^2\cos^2\theta}{LC_n\sin^2\theta + LC_l - LC_l\sin^2\theta - C_D} + \frac{LC_nC_l\sin^2\theta + LC_l^2 - LC_l^2\sin^2\theta - C_DC_l}{LC_n\sin^2\theta + LC_l - LC_l\sin^2\theta - C_D}\} \tag{9}$$

and the required torque to over come the viscous forces produced by the flagellar motion is equal to:

$$T = F_y.A.L \tag{10}$$

$$F_y = -\omega.A\{\frac{(-L.C_n.C_l.\cos^2\theta + C_n.C_D.\cos^2\theta + L.C_l^2.\sin^2\theta.\cos^2\theta)}{L.C_n.\sin^2\theta + L.C_l - L.C_l.\sin^2\theta - C_D} + \frac{-L.C_l.C_n.\sin^2\theta.\cos^2\theta - L.C_n.C_l.\sin^4\theta}{L.C_n.\sin^2\theta + L.C_l - L.C_l.\sin^2\theta - C_D} + \frac{-L.C_l^2.\sin^2\theta + L.C_l^2.\sin^4\theta - C_D.C_l.\sin^2\theta}{L.C_n.\sin^2\theta + L.C_l - L.C_l.\sin^2\theta - C_D}\} \tag{11}$$

The linear velocity of the robot is:

$$U = \omega.A.C_l.\sin\theta\frac{(-C_l + C_n)}{L.C_n.\sin^2\theta + L.C_l - L.C_l.\sin^2\theta - C_D} \tag{12}$$

The efficiency of the robot can be defined as:

$$\eta = \frac{F.U}{T\omega} \tag{13}$$

A non-dimensional analysis [13] of the force, torque and velocity of the system shows that:

$$\frac{T}{\mu\omega L^2} = f_1(\frac{A}{L},\frac{a}{L},\frac{\lambda}{L},\frac{d}{L}) \tag{14}$$

$$\frac{F}{\mu\omega L^2} = f_2(\frac{A}{L},\frac{a}{L},\frac{\lambda}{L},\frac{d}{L}) \tag{15}$$

$$\frac{U}{L\omega} = f_3(\frac{A}{L},\frac{a}{L},\frac{\lambda}{L},\frac{d}{L}) \tag{16}$$

From equations (14) through (16), one can conclude that both efficiency and velocity are functions of geometry only. An optimum design is one which yields the maximum efficiency and velocity. Figure 3 and 4 show how velocity and efficiency change with changing values of different geometrical parameters. An increase in the tail filament diameter will increase both velocity and efficiency. However, the diameter should be small enough for the slender body assumption to hold. A decrease in the size of the body of the robot will also result in increment of both velocity and efficiency. The only constraint on the size of the body is the microscale manufacturing and assembly issues and the size of the components that the designer plans to install in the body of the robot.

IV. EXPERIMENTS

A. Propulsive Force Measurement

To examine the validity of the developed model, an experimental setup is constructed to measure the thrust force produced by a single flagellum at Reynolds numbers comparable to those of microorganisms. To simplify the fabrication and characterization process, utilizing the Buckingham PI theorem, the dimensions of the prototype are scaled up and to compensate for that, the experiment is carried out in silicone oil which is more viscous than water. This way Re number of the scaled up prototype is identical to the Re number of the microscale robot which will be developed in future. According to Buckingham PI theorem, the ratio of $F/(\mu\omega L^2)$ is the same for the scaled up prototype and the microscale robot.

Schematic of the experimental set up is shown in Fig. 5. The head of the prototype is a two-phase stepper motor from Faulhaber®. This motor is 14.5 mm in diameter and 16.5 mm in length. The flagellum is made from steel wire 1.23 mm in diameter. The flagellum has helical diameter of 1.48 cm and pitch of 14.7 mm. The prototype is perpendicularly mounted to a thin steel cantilever beam which is 14 cm long with a cross section of 19.05 by 0.78 mm^2. The tail was submerged in silicone oil with viscosity of 350 cSt from DOW

CORNING®. It was ensured that the tail is fully submerged in oil and is sufficiently far from the walls and the bottom of the oil container. A laser micrometer (LS 3100 from Keyence, Inc.) measures the deflection of the calibrated beam due to the thrust force. Deflection data is used to calculate the thrust force. The experiment was performed for a range of frequencies from 5 Hz to 15 Hz and for two different flagella of the same geometry but different lengths. The dimensions of the two flagella are shown in table 1. Recorded deflection data were passed through a Butterworth filter to eliminate the noise.

Fig. 6. depicts the experimental result for the thrust force generated by the flagellar motion of the prototype in silicon oil. The experimental results are in agreement with theoretical predictions. Thrust force varies linearly with frequency. As shown on Fig. 6, theory suggests that change of the length of the flagellum while all the other geometrical parameters are kept constant, will result in a shift in *y*-axis intercept of the line but the slope doesn't change. This behavior is captured in experiment as well. The uncertainty in the experimental data is due to: (1) The uncertainties associated with the measurement equipment and the user, (2) The uncertainty associated with the calibration process. The difference between the experimental data and the theoretical prediction is due to the fact that coefficients presented in Eq. (6) are for the flagellum with both free ends. The body attached to one end of the flagellum modifies the flow field experienced by the flagellum. This interaction is not considered in RFT. This is probably insignificant for small bodies but for large bodies such as the one used in this experiment, use of more accurate slender-body theory will yield a more accurate results.

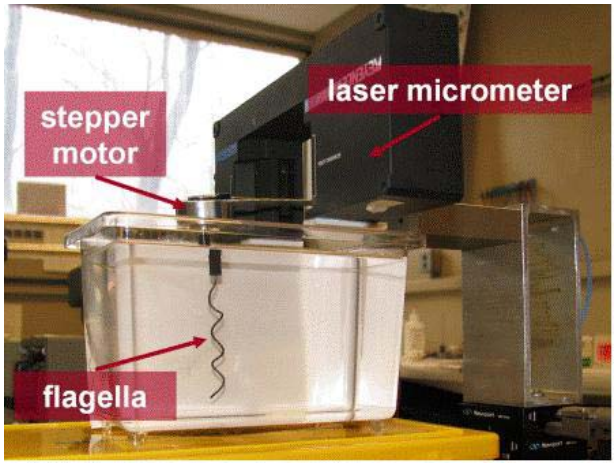

Fig. 5. Experimental setup for propulsive force measurement

Table 1: Dimensions of the swimming microrobot

Half of the thickness of the flagellum, b	0.62 mm
Amplitude of the flagellum, A	0.74 cm
Wavelength of the flagellum, λ	1.47 cm
Length of the flagellum, L_1	5.60 cm
Length of the flagellum, L_2	6.20 cm

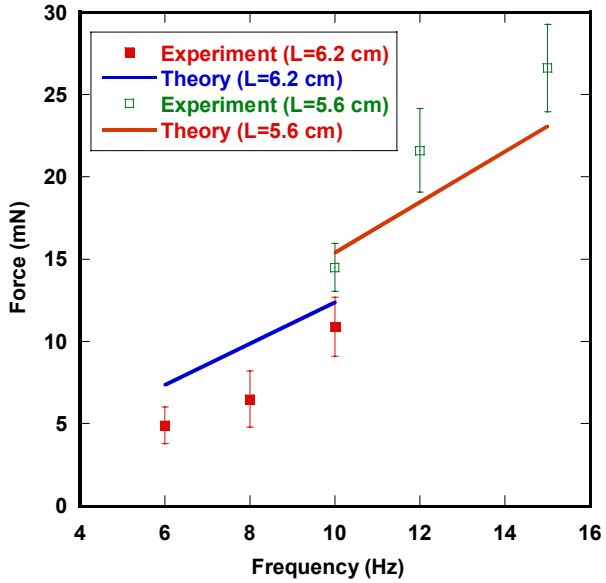

Fig.6. Experimental result for the trust force generated by flagellar propulsion of the prototype in silicone oil

B. *Swimming Robot Prototype*

The first prototype of our swimming robot is depicted in

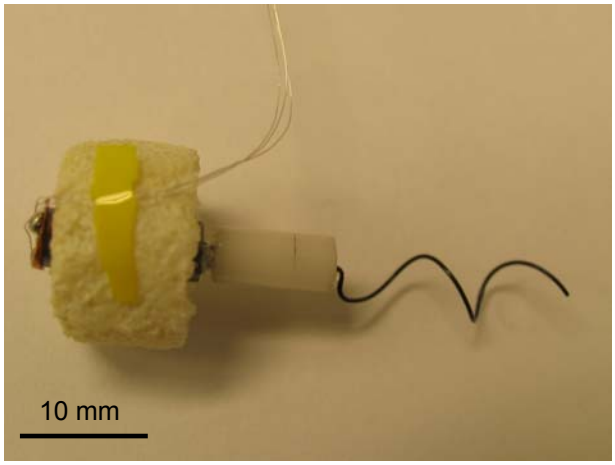

Fig. 7. First prototype of the miniature biomimetic swimming robot

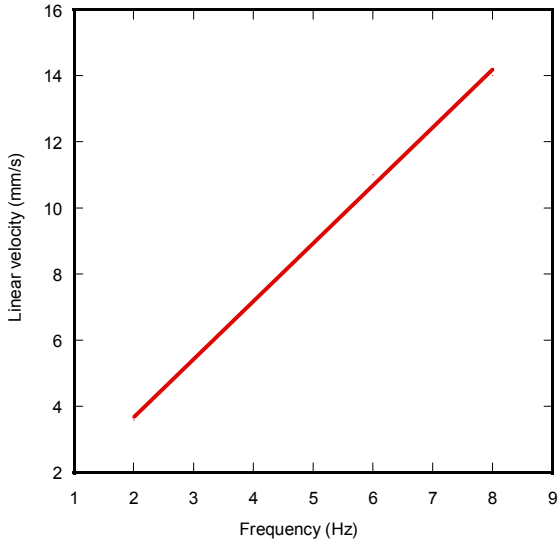

Fig.8. Theoretical prediction for the linear velocity of the biomimetic bacteria robot as a function of frequency of the rotating flagellum

Fig. 7. This prototype weighs 1.85 grams and is 16 mm in diameter and 46 mm in length. It swims in silicone oil with viscosity of 100 cSt from DOW CORNING®. The body of the robot is a brushless DC motor from Myonic, Inc. A Styrofoam jacket is placed on the motor. The dimensions of the jacket are designed so that the robot remains submerged just below the surface of the oil. The flagellum is made from steel wire, 0.42 in diameter. The wavelength of the flagellum is 13 mm, the amplitude is 2.35 mm and the length is about 20 mm.

From the theoretical predictions, the linear velocity of the robot as a function of the angular velocity of the propulsive element is presented in Fig. 8. Currently we are developing the velocity measurement setup to measure the linear velocity of the robot in a more accurate fashion. However, our prototype seems to be moving at speeds close to the predicted values. A video clip of the biomimetic bacteria robot can be seen on our laboratory webpage [14].

V. CONCLUSIONS

Biomimetic propulsion mechanism inspired by prokaryotic flagellar motion is introduced. Analytical model is developed to predict the values for thrust force, required torque, velocity and efficiency. It is shown that all the aforementioned parameters are functions of geometry only. Applying Buckingham PI theorem a scaled-up prototype of the robot was constructed and tested in silicone oil. Experimental results for thrust force are shown to match values predicted by the RFT model. Increasing the number of flagella will enhance both speed and efficiency of the swimming robot. The optimum design of a multi-flagella system in terms of number of flagella and spacing will be investigated.

Another common method of propulsion among microorganisms is known as eukaryotic flagellar motion. Kinematics and dynamic analysis of this motion and comparison between the results of prokaryotic and eukaryotic flagellation would yield an effective design methodology for microscale swimming robots [15].

REFERENCES

[1] T. Fukuda, A. Kawamoto, F. Arai, and H. Matsuura, "Mechanism and Swimming Experiment of Micro Mobile Robot in Water," *Proc. of IEEE Int'l Workshop on Micro Electro Mechanical Systems (MEMS'94),* pp.273-278, 1994.

[2] S. Guo, Y. Hasegaw, T. Fukuda, and K. Asaka, "Fish –Like Underwater Microrobot with Multi DOF," *Proceedings of 200 International Symposium on Micromechatronics and Human Science*, pp. 63-68, 2001.

[3] J. Jung, B. Kim, Y. Tak and J. Park, "Undulatory Tadpole Robot (TadRob) Using Ionic Polymer Metal Composite (IMPC) Actuator," *Proceedings of the 2003 IEEE/RSJ International Conference on Intelligent Robots and Systems*, pp. 2133-2138, 2003.

[4] Y. Zhang, Q. Wang, P. Zhang, X. Wang, T. Mei, "Dynamic Analysis and Experiment of a 3mm Swimming Microrobot," *Proceedings of the 2004 IEEE/RSJ International Conference on Intelligent Robots and Systems* , pp. 1746-1750, 2004.

[5] Honda, T., Arai, K. and Ishiyama, K., "Effect of Micro Machine Shape on Swimming Properties of the Spiral-Type Magnetic Micro-Machine," *IEEE Transaction on Magnetics*, vol. 35, pp. 3688-3690, 1999.

[6] B. Behkam, and M. Sitti, "E. Coli Inspired Propulsion for Swimming Microrobots," *Proceedings of the IMECE 2004*, IMECE2004-59621, Nov. 2004.

[7] J. Edd, S. Payen, B. Rubinsky, M. Stoller, and M. Sitti, "Biomimetic Propulsion for a Swimming Surgical Microrobot," *Proceedings of the 2003 IEEE/RSJ International Conference on Intelligent Robots and Systems*, pp. 2583-2588, 2003.

[8] Darnton, N., Turner, L., Breuer, K., and Berg, H., "Moving Fluid with Bacterial Carpets," *Biophysical Journal*, **86**, pp. 1863-1870, March 2004.

[9] Berg, H., "The Rotary Motor of Bacterial Flagella," *Annual Review of Biochemistry*, **72**, pp. 19-54, 2003.

[10] Leifson, E., "Atlas of Bacterial Flagellation," *Academic Press, New York and London*, 1960.

[11] Johnson, R.E. and Brokaw, C. J., "Flagellar Hydrodynamics: A Comparison between Resistive-Force Theory and Slender-Body Theory," *Biophysics Journal*, vol 25, pp. 113-127.

[12] Brennen, C. and Winet, H., "Fluid Mechanics of Propulsion by Cilia and Flagella," *Annual Review of Fluid Mechanics*, vol. 9, pp. 339-398, 1977.

[13] Fox, R., McDonald, A., and Pritchard, P., "Introduction to Fluid Mechanics," John Wiley & Sons, pp. 273-300, 2004.

[14] http://www.me.cmu.edu/faculty1/sitti/nano/projects/swimming

[15] Behkam, B., and Sitti, M., "Design Methodology for Biomimetic Propulsion of Miniature Biomedical Swimming Robots," *ASME Journal of Dynamic Systems, Measurement and Control* (under review), 2005.